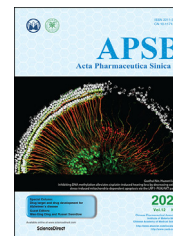




Chinese Pharmaceutical Association
Institute of Materia Medica, Chinese Academy of Medical Sciences

Acta Pharmaceutica Sinica B

www.elsevier.com/locate/apsb
www.sciencedirect.com



ORIGINAL ARTICLE

Structure-guided discovery of potent and oral soluble epoxide hydrolase inhibitors for the treatment of neuropathic pain



Fangyu Du^a, Ruolin Cao^a, Lu Chen^a, Jianwen Sun^a, Yajie Shi^a, Yang Fu^a,
Bruce D. Hammock^b, Zhonghui Zheng^c, Zhongbo Liu^{d,*}, Guoliang Chen^{a,*}

^aKey Laboratory of Structure-Based Drug Design & Discovery of Ministry of Education, School of Pharmaceutical Engineering, Shenyang Pharmaceutical University, Shenyang 110016, China

^bDepartment of Entomology and Nematology and UC Davis Comprehensive Cancer Center, University of California Davis, Davis, CA 95616, USA

^cShandong Xinhua Pharmaceutical Co., Ltd., Zibo 255086, China

^dSchool of Pharmacy, Shenyang Pharmaceutical University, Shenyang 110016, China

Received 10 July 2021; received in revised form 8 September 2021; accepted 15 September 2021

KEY WORDS

Soluble epoxide
hydrolase;
Analgesia;
Synthesis;
Neuropathic pain;
Inhibitor

Abstract Soluble epoxide hydrolase (sEH) is related to arachidonic acid cascade and is over-expressed in a variety of diseases, making sEH an attractive target for the treatment of pain as well as inflammatory-related diseases. A new series of memantyl urea derivatives as potent sEH inhibitors was obtained using our previous reported compound **4** as lead compound. A preferential modification of piperidinyl to 3-carbamoyl piperidinyl was identified for this series *via* structure-based rational drug design. Compound **A20** exhibited moderate percentage plasma protein binding (88.6%) and better metabolic stability *in vitro*. After oral administration, the bioavailability of **A20** was 28.6%. Acute toxicity test showed that **A20** was well tolerated and there was no adverse event encountered at dose of 6.0 g/kg. Inhibitor **A20** also displayed robust analgesic effect *in vivo* and dose-dependently attenuated neuropathic pain in rat model induced by spared nerve injury, which was better than gabapentin and sEH inhibitor (±)-EC-5026. In one word, the oral administration of **A20** significantly alleviated pain and improved the health status of the rats, demonstrating that **A20** was a promising candidate to be further evaluated for the treatment of neuropathic pain.

© 2022 Chinese Pharmaceutical Association and Institute of Materia Medica, Chinese Academy of Medical Sciences. Production and hosting by Elsevier B.V. This is an open access article under the CC BY-NC-ND license (<http://creativecommons.org/licenses/by-nc-nd/4.0/>).

*Corresponding authors: Tel.: +86 13940195895 (Guoliang Chen); +86 13032454403 (Zhongbo Liu).

E-mail addresses: 546265581@qq.com (Zhongbo Liu), chengguoliang@syphu.edu.cn (Guoliang Chen).

Peer review under responsibility of Institute of Materia Medica, Chinese Academy of Medical Sciences and Chinese Pharmaceutical Association.

<https://doi.org/10.1016/j.apsb.2021.09.018>

2211-3835 © 2022 Chinese Pharmaceutical Association and Institute of Materia Medica, Chinese Academy of Medical Sciences. Production and hosting by Elsevier B.V. This is an open access article under the CC BY-NC-ND license (<http://creativecommons.org/licenses/by-nc-nd/4.0/>).

1. Introduction

Neuropathic pain, an intractable pain from somatosensory nervous system damage or disease, which is triggered by pathogenic microorganisms, ischemia, traumatic stimulation, metabolic diseases, drug toxicity, etc., could cause anxiety, depression, even suicide that seriously affect the health and quality of patient's life^{1,2}. Epidemiology statistics from January 1966 to December 2012 showed that approximately 6.9%–10% of the population worldwide suffered from neuropathic pain³. With the increasing trend of population aging, neuropathic pain will become a serious global health problem. Although the pathogenesis of neuropathic pain is still ambiguous, more and more evidence showed that proinflammatory and inflammatory factors play essential role in peripheral and central sensitization of neuropathic pain^{4,5}.

After nerve cell injury, hyperactivated microglia could release a variety of proinflammatory cytokines, including monocyte chemoattractant protein (MCP)-1, tumor necrosis factor (TNF)- α , macrophage inflammatory protein (MIP)-1 α , interleukin (IL)-1 β , IL-6, etc., which induce and maintain neuropathic pain^{6,7}. Currently, drugs for the treatment of patients with neuropathic pain mainly include antiepileptic drugs (such as gabapentin), antidepressants, opioid analgesics, local anesthetics, and nonsteroidal antiinflammatory drugs (NSAIDs), etc.⁸. NSAIDs have poor therapeutic effect on neuropathic pain and display strong adverse events in gastrointestinal or cardiovascular system⁹. Because many patients with neuropathic pain are prescribed opioids to limit their symptoms, there are a lot of incidents with risk of opioid misuse, addiction, tolerance, respiratory depression, nausea and vomiting, etc.¹⁰. Furthermore, antiepileptic drugs also have some central nervous system (CNS) related adverse events, such as drowsiness, dizziness, which show poor therapeutic effect and patient compliance¹¹.

Therefore, it is urgent to develop more effective therapeutic drugs for the management of neuropathic pain with novel mechanisms, strong analgesic effect and without addiction and CNS-related adverse events. Inflammatory cytokines—TNF- α , bradykinin, IL-1 β , IL-6, etc.—serve as a basis in the process of neuropathic pain¹². Therefore, eliminating the production of inflammatory cytokines may offer a new opportunity for the treatment of neuropathic pain^{13,14}.

Arachidonic acid cascade derivatized CYP450 metabolic pathway could oxidize polyunsaturated fatty acid to corresponding epoxy-fatty acids (EpFAs)¹⁵. Endogenous mediators of EpFAs could act through various mechanisms to manage pain as well as inflammation, which was involved in activating peroxisome proliferators-activated receptors (PPARs), reducing endoplasmic reticulum (ER) stress, stabilizing mitochondrial dysfunction, and breaking or reversing endothelial cell dysfunction (ECD)¹⁶. Moreover, EpFAs could also reduce the activation of nuclear factor kappa-B (NF- κ B) by three complementary cellular mechanisms, which is a core mechanism in the anti-inflammatory effect of EpFAs¹⁷. EpFAs could rapidly be hydrolyzed by soluble epoxide hydrolase (sEH) to corresponding pro-inflammatory diol products, leading to inactivation of endogenous active substances *in vivo*¹⁸. sEH inhibitors could stabilize EpFAs and provide a promising therapeutic strategy for pain and inflammatory-related diseases. As summarized in related reviews, this essential cellular mechanism underlies numerous diseases, such as metabolic disease, vascular disease, cytokine storm, etc., and more and more potential therapeutic targets are being gradually disclosed as

the key role of ER stress in related diseases is proved through molecular biology technology^{16,19–21}. Hence, pharmaceutical companies and research institutes involved in the Research & Development of sEH inhibitors have the “problems of the rich” in selecting a promising target and a practical indication from numerous possibilities²¹.

Currently, three sEH inhibitors are moved into the several clinical trials for the treatment of sEH-mediated diseases, as shown in Fig. 1. A great number of published articles revealed the efficacy of sEH inhibitors in regulating hypertension driven by the renin-angiotensin system (RAS)^{22,23}. Therefore, AR-9281 (**1**) developed by Arete Therapeutics was selected as candidate drug to regulate hypertension, which was evaluated in phase II clinical trials²⁴. Inflammation is provoked by various inflammatory leukocytes and cytokines thought to play crucial role in the development process of chronic obstructive pulmonary disease (COPD)²⁵. sEH inhibitors could exert significant protective effects in rat model of COPD²⁵. Therefore, GlaxoSmithKline (GSK) considered COPD as indication as well, and compound GSK-2256294 (**2**), developed by GSK, was evaluated in several phase I clinical trials for the treatment of COPD²⁶. As it is known to all that neuropathic pain still doesn't meet medical demand in clinical practice; however, it is poorly remedied by existing medications. Inspired by the proof that sEH inhibitors could successfully treat severe equine laminitis^{21,27}, EicOsis decided to move it from models into patients. In April 2020, the US Food and Drug Administration (FDA) granted EC-5026 by EicOsis with Fast Track Designation, as a non-addictive alternative to opioid analgesics, for the management of neuropathic pain (NCT04228302), which created favorable conditions for accelerating its clinical development and launch^{21,28}.

Herein, we introduce the discovery and chemical optimization of lead compound **4** based on our previous study²⁹. Through chemical modification of lead compound, we identified racemate molecule that demonstrating strong inhibition of recombinant human sEH (HsEH) *in vitro* assay. A detailed structure–activity relationship (SAR) investigation improved the potency of the single configuration molecule by nearly 4 times, which demonstrated significantly analgesic effect with dose-dependence in spared nerve injury model. Our work supports the development of an orally administered sEH inhibitor for the treatment of neuropathic pain.

2. Results and discussion

2.1. Design strategy

We were devoted to discovering more potent sEH inhibitors containing memantanyl urea and terminal piperidinamide moiety, which were further structurally optimized from previously reported compound²⁹. We visualized those new compounds might demonstrate low melting point, and good water solubility with favorable pharmacokinetic (PK) properties. To facilitate the design of new sEH inhibitors, we further analyzed the binding modes of lead compound **4** with sEH protein (PDB ID: 3WKE) through Discovery Studio 2016 software, as disclosed in Fig. 2. Binding surface results displayed that piperidinyl moiety of compound **4** was exposed to solvent cavity, which offered several opportunities to increase potency of inhibitors as there were several extra amino acid residues situated in the solvent cavity of sEH. In addition, substitution at piperidinyl moiety provided an

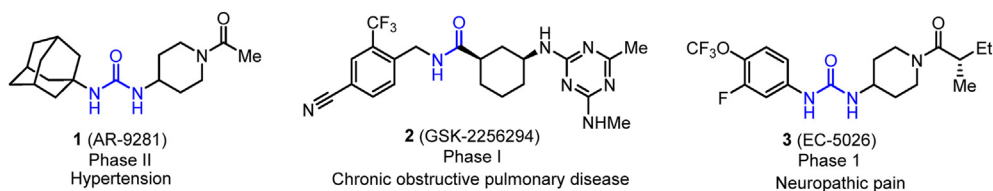


Figure 1 Chemical structures of sEH inhibitors in clinic trials.

opportunity to introduce polar functional groups, which was contributed to modulating the physicochemical properties of the compounds. Therefore, memantyl urea and benzamide groups were retained, carboxyl was introduced to piperidiny moiety at C3 and C4 position, which was further derivatized with amines or alcohol leading to target compounds (Scheme 1).

In vitro biological activity screening showed that substituents at C3 position of piperidiny moiety demonstrated better inhibitory effect than C4 position. Amongst, compound with carbonyl displayed strong inhibitory potency on sEH. Considering that lead compound **4** was easily metabolized *in vitro* and *in vivo*; therefore, F and Cl atoms were respectively introduced to central phenyl group to improve the metabolic stability (Scheme 1). Meanwhile, these compounds are featured with *para*-disubstituted with strong molecular symmetry. The introduction of halogen atoms at phenyl group could reduce structural symmetry, which was beneficial to reduce melting point and improve solubility. The introduction of halogen atoms afforded the most potency compounds with good physical properties. Substituents at C3 position of piperidiny moiety include a chiral carbon atom, biological activity assay screening revealed that *S*-configurational molecule was a more potent sEH inhibitor than *R*-configuration by nearly 2 times. According to

above results, compound with *S*-configuration and F substituent was obtained, which demonstrated strong inhibitory potency on sEH (Scheme 1).

In consideration of chemical character of piperidiny as well as significant inhibitory effects of derivatives *in vitro*, piperidiny was respectively replaced with 4-aminopiperidiny and piperaziny, then further acylated with different acids to obtain target compounds **B1–B8** and **C1–C8**, respectively. Referring to the compound **A20**, we replaced 4-aminopiperidiny with (*S*)-3-aminopiperidiny, and introduced F atom at phenyl group, leading to compound **B9**, as shown in Scheme 1.

2.2. Chemistry

The strategy adopted for the synthesis of compound **A1** (Scheme 2) started with commercially available *para*-nitrobenzoyl chloride, which underwent acylation with piperidine-4-carboxylic acid to provide compound **6**. Reduction of **6** using 5% Pd-C at H₂ atmosphere under mildly condition provided **7**. Subsequent acylation of the amino group present in **7** with phenyl chloroformate, and resulting key intermediate **8** was nucleophilic substituted with memantine to give **A1**. Esterification of the carboxyl of **A1** with EtOH in the presence of SOCl₂ provided compound **A2**.

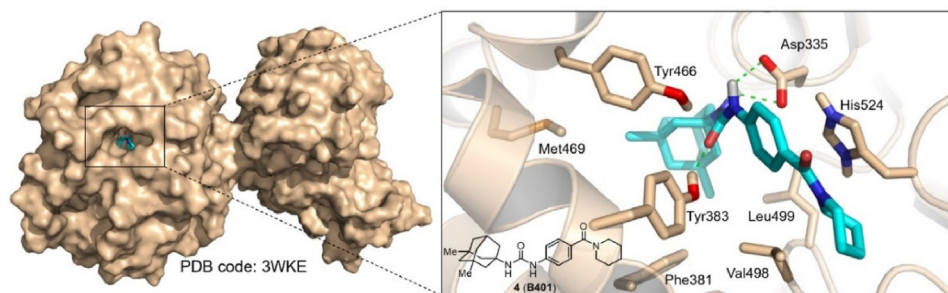
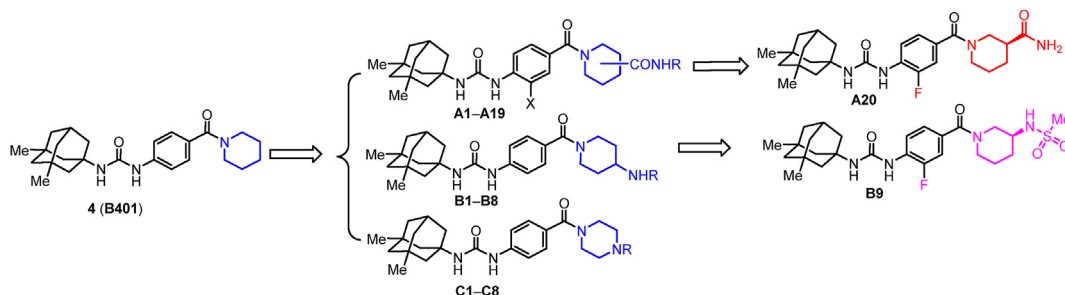


Figure 2 Docked pose of compound **4** in blue bound to sEH (PDB ID: 3WKE).



Scheme 1 Design strategy based on lead compound **4**.

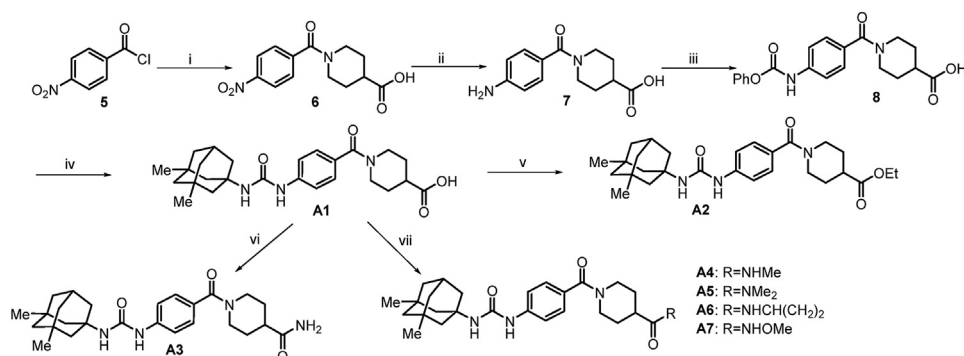
Chlorination of **A1** with SOCl_2 in THF cleanly afforded the acyl chloride intermediate (not shown). Subsequent acylation (ammonia, THF, 0°C) yield compound **A3**. Commercially available amines were then coupled to the compound **A1** with the assistance of 1-ethyl-3-(3-dimethylaminopropyl)carbodiimide hydrochloride (EDCI) and 1-hydroxybenzotriazole (HOBt) in DCM solution to give **A4–A7**. Compounds **A8–A14** were obtained in similar route starting from commercially available piperidine-3-carboxylic acid, as shown in Scheme 3.

Halogen substituted compounds **A15** and **A16** were synthesized as exhibited in Scheme 4. Chlorination of 3-fluoro-4-nitrobenzoic acid **12** and 3-chloro-4-nitrobenzoic acid **13** with SOCl_2 in THF cleanly afforded the corresponding acyl chloride intermediate (not shown). Subsequent acylation with ethyl piperidine-3-carboxylate respectively yield compounds **14** and **15**. It is noteworthy that reduction of intermediates **14** and **15** containing halogen atom using 5% Pd-C at H_2 atmosphere condition didn't provide corresponding target compounds, but leading to side dehalogenation reaction. Therefore, anilines **16** and **17** were obtained in good to excellent yields *via* reduction of nitro intermediates **14** and **15** in the presence of $\text{Fe}/\text{NH}_4\text{Cl}$ under standard conditions. Moreover, phenyl chloroformate has been firstly utilized for urea formation, which was similar with Schemes 2 and 3. However, corresponding intermediates containing halogen atom couldn't react with memantine. Hence, we replaced phenyl chloroformate with triphosgene (BTC) to obtain urea

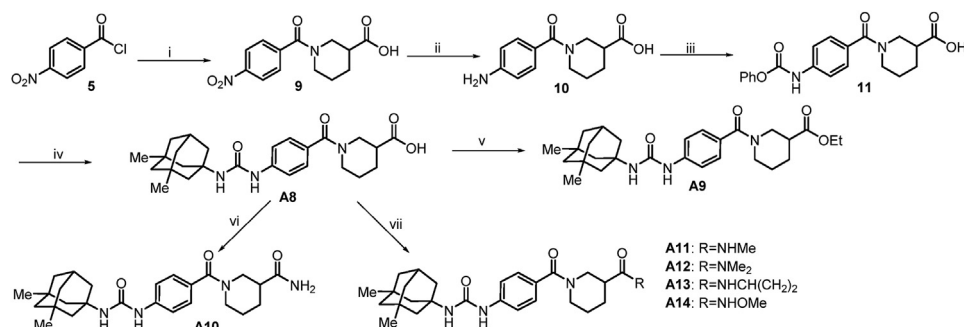
compounds. Amino groups in **16** and **17** were transformed to the corresponding isocyanate (not shown) in the presence of BTC, and then reacted with memantine to respectively give compounds **18** and **19**, which were hydrolyzed under basic conditions to affording the desired acid intermediates. Chlorination of the acids **20** and **21** using SOCl_2 , followed by coupling with ammonia, generated the corresponding target compounds **A15** and **A16**.

The preparation of compound **A17** started with the previously described **A1** (Scheme 4). Esterification of the carboxyl of **A1** with MeOH in the presence of SOCl_2 provided **22**. Subsequent aminolysis of the methyl ester in hydroxylamine aqueous afforded **A17**.

The synthesis of chiral compounds **A18** and **A19** (Scheme 5) was accomplished *via* acylation of commercially available (*R*)-ethyl piperidine-3-carboxylate and (*S*)-ethyl piperidine-3-carboxylate with 4-nitrobenzoyl chloride to give **23** and **24**. Hydrogenation reduction of the nitro group in compounds **23** and **24** yielded the amino intermediates. Subsequent acylation of the amino group present in **25** and **26** with phenyl chloroformate, and resulting key intermediates **27** and **28** were nucleophilic substituted with memantine to respectively give **29** and **30**, followed by hydrolysis of ester under basic condition afforded **31** and **32**. Chlorination of the acids **31** and **32** using SOCl_2 , followed by coupling with ammonia, generated the corresponding target compounds **A18** and **A19**.



Scheme 2 Synthetic route to compounds **A1–A7**. Reactions and conditions: i) piperidine-4-carboxylic acid, K_2CO_3 , THF/ H_2O ; (ii) H_2 (g), 5% Pd-C, EtOH, 60°C , 12 h; (iii) K_2CO_3 , PhOCOCl , THF, $0^\circ\text{C} \rightarrow \text{rt}$; iv) memantine, Et_3N , THF, 75°C , 8 h; v) SOCl_2 , EtOH, $0^\circ\text{C} \rightarrow \text{reflux}$, 2 h; vi) (1) SOCl_2 , DMF, THF; (2) NH_3 (g), THF; vii) amines, EDCI, HOBt, Et_3N , DCM, rt.



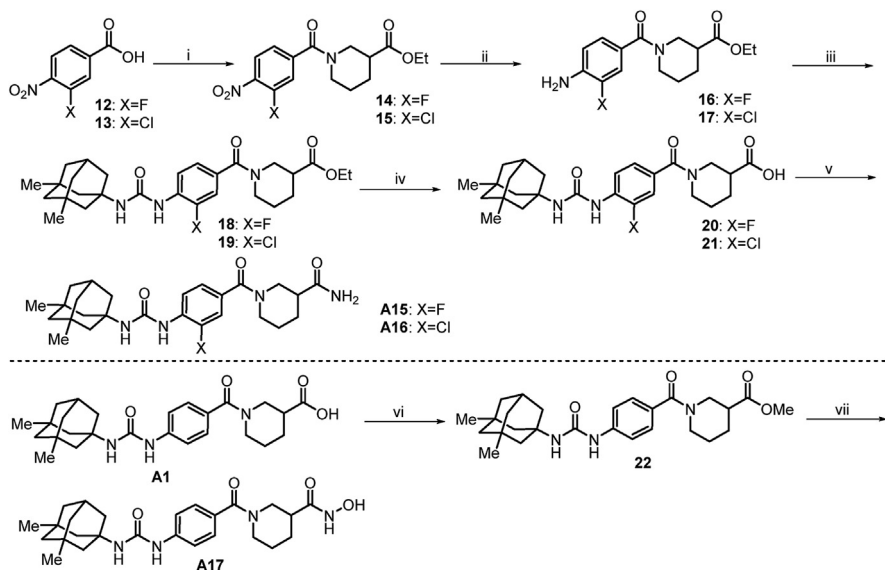
Scheme 3 Synthetic route to compounds **A8–A14**. Reactions and conditions: i) piperidine-3-carboxylic acid, K_2CO_3 , THF/ H_2O ; (ii) H_2 (g), 5% Pd-C, EtOH, 60°C , 12 h; (iii) K_2CO_3 , PhOCOCl , THF, $0^\circ\text{C} \rightarrow \text{rt}$; iv) memantine, Et_3N , THF, 75°C , 8 h; v) SOCl_2 , EtOH, $0^\circ\text{C} \rightarrow \text{reflux}$, 2 h; vi) (1) SOCl_2 , DMF, THF; (2) NH_3 (g), THF; vii) amines, EDCI, HOBt, Et_3N , DCM, rt.

The synthesis of compounds **A20** and **A21** (Scheme 6) was accomplished starting from 3-fluoro-4-nitrobenzoic acid. Chlorination of 3-fluoro-4-nitrobenzoic acid **12** with SOCl_2 in THF cleanly afforded the corresponding acyl chloride intermediate (not shown). Subsequent acylation with (*S*)-ethyl piperidine-3-carboxylate or (*R*)-ethyl piperidine-3-carboxylate yield compounds **33** and **34**. Anilines **35** and **36** were prepared in excellent yield *via* reduction of nitro compounds **33** and **34** in the presence of $\text{Fe}/\text{NH}_4\text{Cl}$ under standard conditions. Amino group in **35** and **36** was transformed to the corresponding isocyanate (not shown) in the presence of BTC, and then reacted with memantine to give compounds **37** and **38**, which after hydrolysis under basic conditions gave the desired intermediate acids **39** and **40**. Chlorination of the acids **39** and **40** using SOCl_2 , followed by coupling with ammonia, generated the desired compounds **A20** and **A21**.

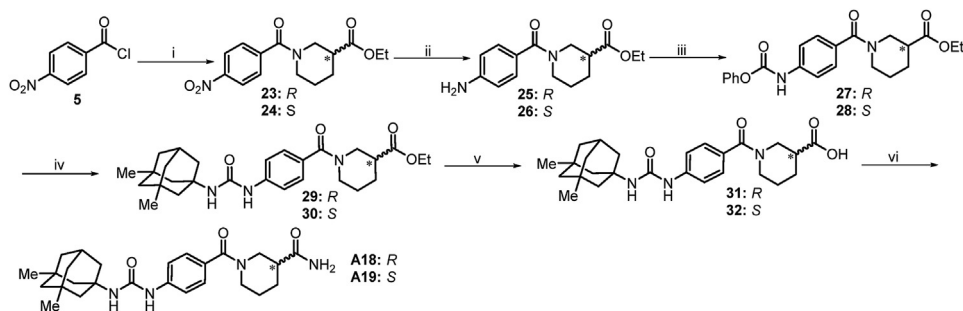
The preparation of compound **B1** (Scheme 7) started with *para*-nitrobenzoyl chloride, which underwent acylation with *tert*-butyl piperidin-4-ylcarbamate to provide compound **41**. Reduction

of **41** using 5% Pd-C at H_2 atmosphere under mildly condition provided **42**. Subsequent acylation of the amino group present in **42** with phenyl chloroformate, and resulting key intermediate **43** was nucleophilic substituted with memantine to give **44**. Removal of the Boc group in **44** with diluted trifluoroacetic acid (TFA) furnished the amine **B1** quantitatively. Subsequent acylation of the amino group present in **B1** with commercially available methanesulfonyl chloride, acetyl chloride and propionyl chloride to give corresponding compounds **B2–B4**. Then, commercially available acids (not shown) were then coupled to the compound **B1** with the assistance of EDCI and HOBt in DCM solution to give **B5–B7** and **45**. Treatment of **45** with TFA deprotected the Boc group to give compound **B8**.

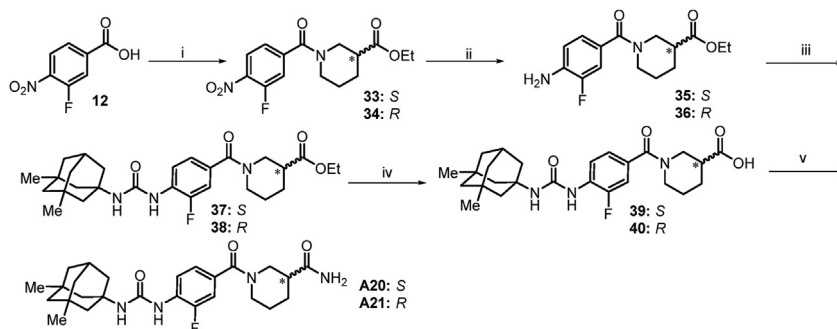
The synthesis of compound **B9** (Scheme 8) was accomplished using 3-fluoro-4-nitrobenzoic acid as starting material. Chlorination of 3-fluoro-4-nitrobenzoic acid **12** with SOCl_2 in THF cleanly afforded the corresponding acyl chloride intermediate (not shown). Subsequent acylation with *tert*-butyl (*S*)-piperidin-3-ylcarbamate



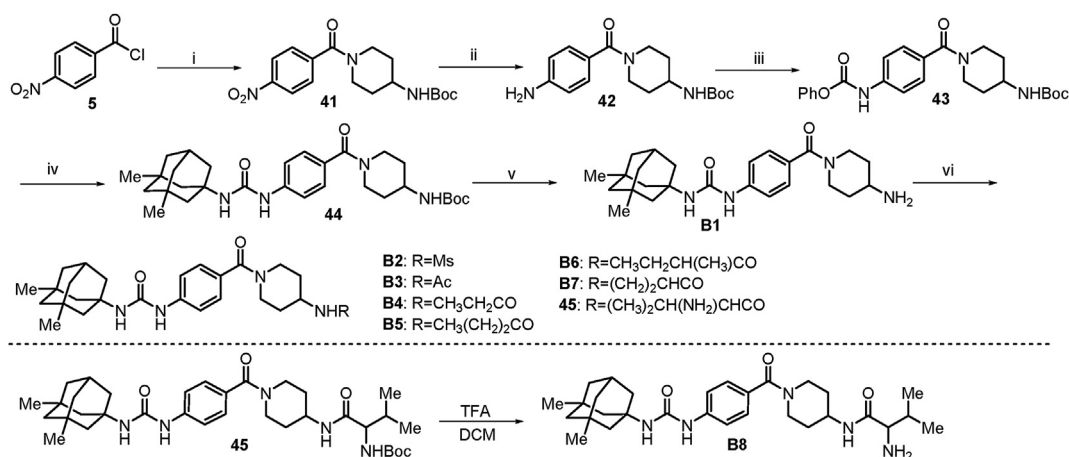
Scheme 4 Synthetic route to compounds **A15–A17**. Reactions and conditions: i) (1) SOCl_2 , DMF, THF, $0^\circ\text{C} \rightarrow \text{rt}$; (2) ethyl piperidine-3-carboxylate, Et_3N , THF, $0^\circ\text{C} \rightarrow \text{rt}$; ii) Fe , NH_4Cl , $\text{EtOH}/\text{H}_2\text{O}$, 70°C ; iii) (1) BTC, Et_3N , DCM, $0^\circ\text{C} \rightarrow \text{reflux}$; (2) memantine, Et_3N , DCM, $0^\circ\text{C} \rightarrow \text{rt}$; iv) (1) NaOH , H_2O , EtOH ; (2) Conc. HCl ; v) (1) SOCl_2 , DMF, THF, $0^\circ\text{C} \rightarrow \text{rt}$; (2) NH_3 (g), THF, $0 \rightarrow \text{rt}$; vi) SOCl_2 , MeOH, $0^\circ\text{C} \rightarrow \text{reflux}$, 2 h; vii) 50% (w/w) NH_2OH solution, 1 mol/L NaOH , MeOH, 0°C .



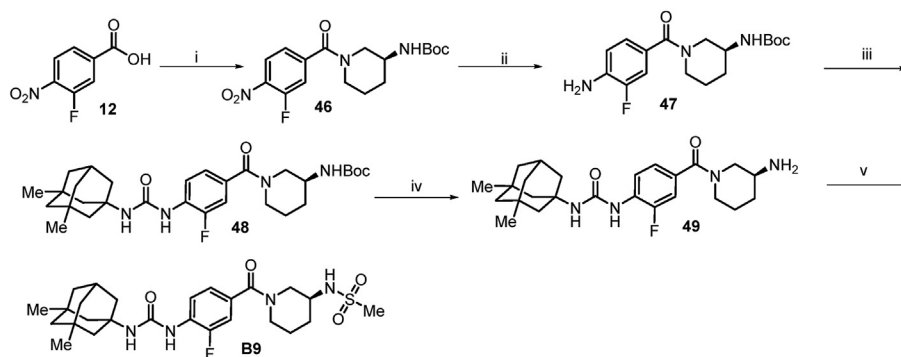
Scheme 5 Synthetic route to compounds **A18** and **A19**. Reactions and conditions: i) *R*- or *S*-ethyl piperidine-3-carboxylate, Et_3N , THF, $0^\circ\text{C} \rightarrow \text{rt}$; ii) H_2 (g), 5% Pd-C, EtOH , 60°C , 12 h; iii) K_2CO_3 , PhOCOCl , THF, $0^\circ\text{C} \rightarrow \text{rt}$; iv) memantine, Et_3N , THF, 75°C , 8 h; v) (1) NaOH , H_2O , EtOH ; (2) Conc. HCl ; vi) (1) SOCl_2 , DMF, THF; (2) NH_3 (g), THF.



Scheme 6 Synthetic route to compound **A20** and **A21**. Reactions and conditions: i) (1) SOCl_2 , DMF, THF, $0^\circ\text{C} \rightarrow 60^\circ\text{C}$; (2) (*S*)-ethyl piperidine-3-carboxylate or (*R*)-ethyl piperidine-3-carboxylate, Et_3N , THF, $0^\circ\text{C} \rightarrow \text{rt}$; ii) Fe, NH_4Cl , $\text{EtOH}/\text{H}_2\text{O}$, 70°C ; iii) (1) BTC, Et_3N , DCM, $0^\circ\text{C} \rightarrow \text{reflux}$; (2) memantine, Et_3N , DCM, $0^\circ\text{C} \rightarrow \text{rt}$; iv) (1) NaOH, H_2O , EtOH ; (2) Conc. HCl; v) (1) SOCl_2 , DMF, THF, $0^\circ\text{C} \rightarrow \text{rt}$; (2) NH_3 (g), THF, $0^\circ\text{C} \rightarrow \text{rt}$.



Scheme 7 Synthetic route to compounds **B1–B8**. Reactions and conditions: (i) *tert*-butyl piperidin-4-yl-carbamate, Et_3N , THF, $0^\circ\text{C} \rightarrow \text{rt}$, 6 h; (ii) H_2 (g), 5% Pd-C, EtOH , 60°C , 12 h; (iii) K_2CO_3 , PhOCOCl , THF, $0^\circ\text{C} \rightarrow \text{rt}$, 7 h; (iv) memantine, Et_3N , THF, 75°C , 8 h; v) TFA, DCM, $0^\circ\text{C} \rightarrow \text{rt}$, 2 h; vi) (a) corresponding acyl chlorides, Et_3N , DCM; or (b) corresponding acids, EDCI, HOBT, Et_3N , DCM, rt .

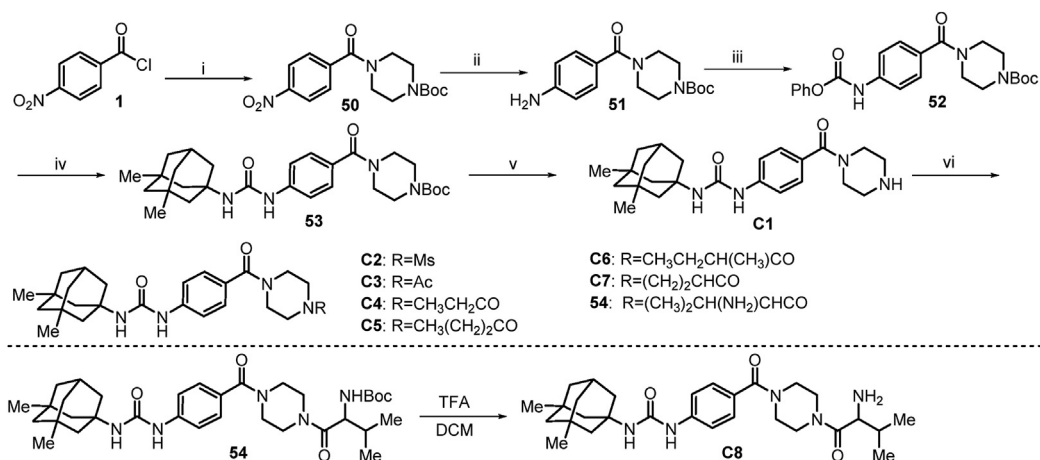


Scheme 8 Synthetic route to compound **B9**. Reactions and conditions: i) (1) SOCl_2 , DMF, THF, $0 \rightarrow 60^\circ\text{C}$; (2) *tert*-butyl (*S*)-piperidin-3-yl-carbamate, Et_3N , THF, $0^\circ\text{C} \rightarrow \text{rt}$; ii) Fe, NH_4Cl , $\text{EtOH}/\text{H}_2\text{O}$, 70°C ; iii) (1) BTC, Et_3N , DCM, $0^\circ\text{C} \rightarrow \text{reflux}$; (2) memantine, Et_3N , DCM, $0^\circ\text{C} \rightarrow \text{rt}$; iv) TFA, DCM, $0^\circ\text{C} \rightarrow \text{rt}$; v) MsCl, Et_3N , DCM, $0^\circ\text{C} \rightarrow \text{rt}$.

yield compound **46**. Aniline **47** was prepared in excellent yield *via* reduction of nitro compound **46** in the presence of Fe/ NH_4Cl under standard conditions. Amino group in **47** was transformed to isocyanate (not shown) in the presence of BTC, and then reacted with memantine to give compound **48**. Removal of the Boc group in **48**

with diluted TFA furnished the amine **49** quantitatively. Subsequent acylation of the amino group present in **49** with commercially available methanesulfonyl chloride to give compound **B9**.

The preparation of compound **C1** (Scheme 9) started with 4-nitrobenzoyl chloride, which underwent acylation with *tert*-butyl



Scheme 9 Synthetic route to compounds **C1**–**C8**. Reactions and conditions: (i) *tert*-butyl piperazine-1-carboxylate, Et₃N, THF, 0 °C → rt, 6 h; (ii) H₂ (g), 5% Pd-C, EtOH, 60 °C, 12 h; (iii) K₂CO₃, PhOCOCl, THF, 0 °C → rt, 7 h; (iv) memantine, Et₃N, THF, 75 °C, 8 h; (v) TFA, DCM, 0 °C → rt, 2 h; (vi) (a) corresponding acyl chlorides, Et₃N, DCM; or (b) corresponding acids, EDCI, HOBT, Et₃N, DCM, rt.

piperazine-1-carboxylate to provide compound **50**. Reduction of **50** using 5% Pd-C at H₂ atmosphere under mildly condition provided **51**. Subsequent acylation of the amino group present in **51** with phenyl chloroformate, and resulting key intermediate **52** was nucleophilic substituted with memantine to give **53**. Removal of the Boc protecting group in **53** with diluted TFA furnished the amine **C1** quantitatively. Subsequent acylation of the amino group present in **C1** with commercially available methanesulfonyl chloride, acetyl chloride and propionyl chloride to give corresponding compounds **C2**–**C4**. Then, commercially available acids (not shown) were then coupled to the compound **C1** with the assistance of EDCI and HOBT in DCM solution to give **C5**–**C7** and **54**. Treatment of **54** with TFA deprotected the Boc group to give compound **C8**.

2.3. Molecular docking

We used computer aided drug design to simulate possible binding modes of compounds **A20** and **B9** in the active pocket of sEH protein (PDB ID: 3WKE) through Discovery Studio 2016 software, as depicted in Fig. 3. Compounds **A20**, **B9** and *t*-AUCB adopt the same conformation to bind to the sEH active pocket (Fig. 3A). The urea group forms hydrogen bonds with catalytic triad constituted with backbones of residues Asp335, Tyr383, and Tyr466 (Fig. 3B and C). The F atom of the phenyl group makes halogen bond with Phe267. The phenyl group of **A20** and **B9** not only binds in a hydrophobic cavity but also makes key π -cation interaction with residues of His524. Carbamoyl moiety of **A10** and methanesulfonamide group of **B9** extend to the solvent exposure area, which form hydrogen

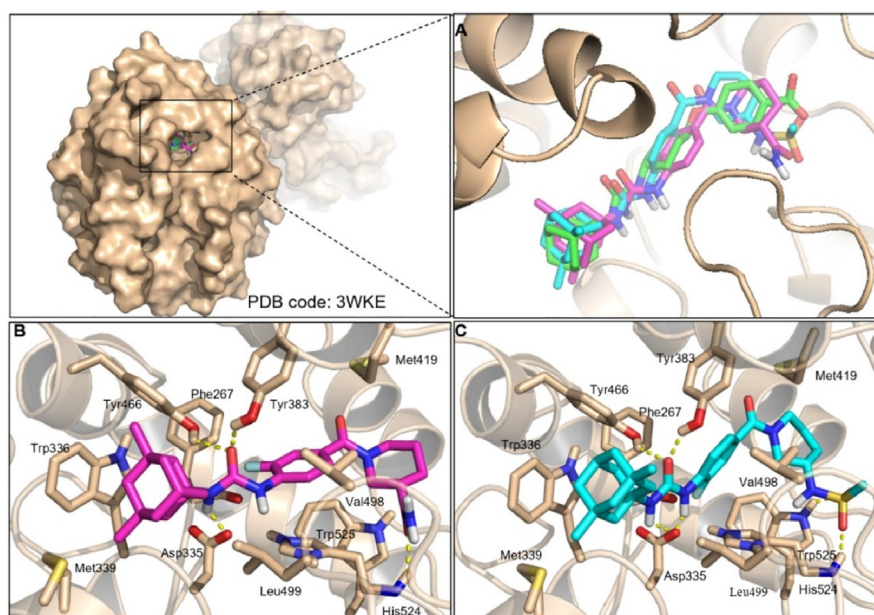
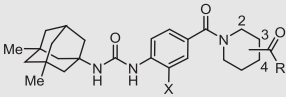


Figure 3 Molecular simulation of compounds **A20** and **B9** bound to sEH (PDB ID: 3WKE). (A) showed docked poses of compounds **A20** (purple), **B9** (blue) and *t*-AUCB (green) in sEH binding pocket. (B) indicated sEH bound to compound **A20** in purple. (C) displayed sEH bound to compound **B9** in blue. Hydrogen bond was showed as dash in yellow.

Table 1 Exploration of pipercolic acid derivatives SAR.


Compd.	Structure	Subst.	IC ₅₀ (nmol/L) ^a	cLogP ^b	LLE ^c
A1	X = H, R ₁ = OH	4	>1000	3.017	—
A2	X = H, R ₁ = OEt	4	0.44 ± 0.26	3.591	5.762
A3	X = H, R ₁ = NH ₂	4	0.99 ± 0.18	2.390	6.616
A4	X = H, R ₁ = NHMe	4	0.74 ± 0.23	2.595	6.538
A5	X = H, R ₁ = NMe ₂	4	0.75 ± 0.54	2.801	6.321
A6	X = H, R ₁ = NHCH(CH ₂) ₂	4	1.14 ± 0.77	3.085	5.859
A7	X = H, R ₁ = NHOMe	4	0.92 ± 0.25	2.441	6.596
A8	X = H, R ₁ = OH	3	0.42 ± 0.36	3.152	6.222
A9	X = H, R ₁ = OEt	3	0.21 ± 0.19	3.726	5.942
A10	X = H, R ₁ = NH ₂	3	0.25 ± 0.11	2.525	7.076
A11	X = H, R ₁ = NHMe	3	0.45 ± 0.39	2.730	6.614
A12	X = H, R ₁ = NMe ₂	3	0.37 ± 0.21	2.936	6.499
A13	X = H, R ₁ = NHCH(CH ₂) ₂	3	0.36 ± 0.23	3.220	6.219
A14	X = H, R ₁ = NHOMe	3	0.34 ± 0.22	2.576	6.887
A15	X = F, R ₁ = NH ₂	3	0.15 ± 0.13	2.730	7.094
A16	X = Cl, R ₁ = NH ₂	3	0.18 ± 0.11	3.189	6.561
A17	X = H, R ₁ = NHOH	3	0.39 ± 0.29	2.537	6.868
A18	X = H, R ₁ = NH ₂	3(<i>R</i>)	0.31 ± 0.30	2.525	7.683
A19	X = H, R ₁ = NH ₂	3(<i>S</i>)	0.12 ± 0.10	2.525	6.988
A20	X = F, R ₁ = NH ₂	3(<i>S</i>)	0.06 ± 0.05	2.730	7.487
A21	X = F, R ₁ = NH ₂	3(<i>R</i>)	0.08 ± 0.03	2.730	7.367
4	—	—	0.40 ± 0.25	3.832	5.566
(±)-EC-5026	—	—	0.09 ± 0.02	4.227	5.825
AR-9281	—	—	13.8	1.300	6.570

^aThe cell-free IC₅₀ values are recorded on HsEH protein based on biochemical method. The IC₅₀ values were expressed as mean ± standard error of mean (SEM).

^bDiscovery Studio 2016 software was used to predict clogP values.

^cLigand lipophilicity efficiency (LLE) was calculated by following equation: LLE = pIC₅₀ - clogP.

bond with His524, respectively. In addition, methanesulfonamide group of **B9** makes extra hydrogen bond with Trp525. These may explain why compounds **A10** and **B9** could enhance inhibitory potency comparing to lead compound **4**. The methyl groups of the memantyl moiety extend to a hydrophobic pocket formed by the backbones of residues Trp336 and Met339. These possibly binding modes suggest that the piperidinamide tail group may be contributing strongly to the binding affinity for the sEH protein.

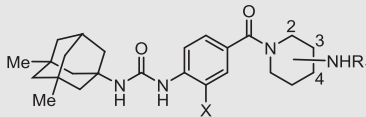
2.4. Structure–activity relationships of series derivatives

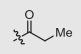
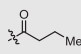
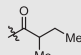
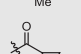

The memantyl urea moiety has been shown to be promising with respect to the sEH inhibitory effect of compounds. Cell-free recombinant HsEH IC₅₀ assays based on biochemical method were performed on series compounds³⁰, and the results of these experiments were compared against the cell-free IC₅₀ of lead compound **4**. These data were provided in Tables 1–3.

According to the activities shown in Table 1, it appears that substituent at C3 position was beneficial and the terminal amide or ester moiety was fundamental for activity retention. Inhibitory potency on sEH of compounds substituted at C3 position (**A8**–**A14**) was slightly better than substituents at C4 position (**A1**–**A7**). Amongst, compound **A1** substituted with 4-COOH group displayed lowest inhibitory potency, with IC₅₀ value > 1000 nmol/L. Replacing carboxyl with amide or ester resulted in improving potency significantly. The best results were achieved with the ethyl ester-containing compound **A9**, showing IC₅₀ value of 0.21 nmol/L.

Among the different primary amide (–NH₂ **A10**), secondary amides (–NHMe **A11**, cyclopropylamine **A13**, NHOMe **A14**) and tertiary amide (–NMe₂ **A12**) examined, the best results were obtained with the carbamoyl-containing compound **A10**, showing IC₅₀ value of 0.25 nmol/L. Compound containing hydroxamic acid group (**A17**) displayed similar potency with carboxyl compound (**A8**) with IC₅₀ values of 0.39 and 0.42 nmol/L. Although compound **A9** was more potency than **A10** in the inhibition of sEH *in vitro*, **A9** was more easily metabolized by hydrolysis than **A10** according to chemical stability. In addition, compound **A10** possessed higher ligand lipophilicity efficiency (LLE)³¹. Accordingly, we selected compound **A10** as the template for further optimization.

Next, we further modified the phenyl linker to improve potency of compounds. Excitingly, replacing the H atom at X with F and Cl resulted in compounds **A15** and **A16**, which displayed about 2.5- and 2-fold potency improvements comparing to **A10** with IC₅₀ values of 0.15 and 0.18 nmol/L. In addition, substitution with halogen atom might prevent the metabolism of the phenyl group, and improve physical properties, *e.g.*, melting point and solubility. Then, exploration on the chirality center of C3 position in **A10** would be expected to further improve the potency. The two enantiomers **A18** (*R*) and **A19** (*S*) were respectively synthesized to determine the chiral preference for sEH inhibition. It was observed that the inhibitory potency of (*S*) **stereoisomer** (**A19**) was 2-fold stronger than (*R*) enantiomer (**A18**) with IC₅₀ values of 0.12 and 0.31 nmol/L, respectively. Taken together, data showed that (*S*)-carbamoyl substituent at C3 position of piperidinyl

Table 2 Exploration of aminopiperidine derivatives SAR.


Compd.	Structure	Subst.	IC ₅₀ (nmol/L) ^a	cLogP ^b	LLE ^c
B1	X = H, R ₁ = H	4	2.14 ± 1.19	2.337	6.332
B2	X = H, R ₁ = Ms	4	0.79 ± 0.30	1.923	7.178
B3	X = H, R ₁ = Ac	4	1.36 ± 0.98	2.132	6.734
B4	X = H, R ₁ = 	4	0.60 ± 0.37	2.799	6.420
B5	X = H, R ₁ = 	4	0.50 ± 0.39	3.255	6.043
B6	X = H, R ₁ = 	4	0.45 ± 0.21	3.718	5.629
B7	X = H, R ₁ = 	4	0.60 ± 0.44	2.890	6.330
B8	X = H, R ₁ = 	4	0.45 ± 0.40	2.498	6.846
B9	X = F, R ₁ = Ms	3	0.11 ± 0.03	2.593	7.347
4	—	—	0.40 ± 0.25	3.830	5.570
(±)-EC-5026	—	—	0.09 ± 0.02	4.227	5.825
AR-9281	—	—	13.8	1.300	6.570

^aThe cell-free IC₅₀ values are recorded on HsEH protein based on biochemical method. The IC₅₀ values were expressed as mean ± standard error of mean (SEM).

^bDiscovery Studio 2016 software was used to predict clogP values.

^cLigand lipophilicity efficiency (LLE) was calculated by following equation: LLE = pIC₅₀ - clogP.

moiety and F substituent at phenyl linker (**A20**) was the optimal combination, not only providing strong inhibitory potency against the HsEH (IC₅₀ = 0.06 nmol/L) but also demonstrating better metabolic stability and high LLE. Similar potency improvement (**A21**) was observed at enantiomer of **A20**, which was slightly weaker than **A20** against HsEH, with IC₅₀ values of 0.08 and 0.06 nmol/L.

Next, we performed structural modifications by changing the piperidinyl moiety of the lead compound **4**. As shown in **Table 2**, replacing piperidinyl moiety (**4**) with 4-aminopiperidinyl (**B1**) resulted in decreasing inhibitory potency with IC₅₀ value of 2.14 nmol/L. The incorporation of amides tail at the 4-aminopiperidinyl moiety resulted in compounds (**B2–B8**) with quite potent biochemical activity against HsEH. Among them, compound **B3**, bearing the acetyl group yielded the lowest potency with IC₅₀ value of 1.36 nmol/L. Furthermore, methanesulfonamide group increased both potency and LLE, which might improve solubility and give more favorable physicochemical properties. Taken together, replacing 4-aminopiperidinyl with (*S*)-3-aminopiperidinyl and introducing of F atom at phenyl linker resulted in more potent inhibitor **B9** with IC₅₀ value of 0.11 nmol/L, which displayed higher LLE (7.347) than lead compound **4** (5.570).

As shown in **Table 3**, replacing piperidinyl moiety (**4**) with piperazinyl moiety (**C1**) resulted in significantly decreasing inhibitory potency with IC₅₀ value > 1000 nmol/L. The incorporation of amides tail at the NH group of piperazinyl moiety resulted in compounds (**C2–C8**) with high inhibitory potency against HsEH. Among them, compound **C2**, bearing the methanesulfonamide group yielded the best potency with IC₅₀ value of 0.73 nmol/L and increased favorable LLE (7.269). These data concluded that piperazinyl derivatives demonstrated weaker

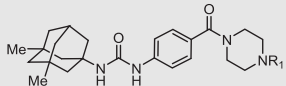
potency than compound **4**, and other biological screenings weren't further evaluated *in vitro* and *in vivo*. Therefore, considering the potency and drug like properties, compounds **A10** and **A20** were selected as candidate compounds for further evaluated *in vivo*.

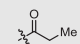
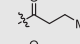
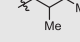
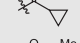
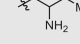
2.5. Microsomal stability

To determine the microsomal stability, preliminary microsomal stability studies (see **Table 4**) were carried out for the compounds **A10** and **A20**. Both compounds displayed better metabolic stability than lead compound **4** *in vitro*. Compound **A10** could remain in human and rat liver microsomes, with half-life (*t*_{1/2}) of 69 min and 84 min. Excitingly, **A20** displayed best microsomal stability for both human and rat species than compound **A10** and lead compound **4**, with *t*_{1/2} of 174 and 120 min, respectively. The results showed that F atom substituent could increase metabolic stability. Based on melting point and bioavailability, the F atom substitution (**A20**) further reduced the melting point and improved LLE, and **A20** indicated most promise as it displayed the highest LLE.

2.6. Pharmacokinetic study *in vivo*

Considering to their good inhibitory potency, as well as suitable metabolic stability *in vitro*, the pharmacokinetics profile of **A10** and **A20** were further evaluated. After oral (*po*) and intravenous (*iv*) administration at a single dose, blood levels were analyzed to 12 or 24 h and pharmacokinetic parameters were shown in **Table 5**. The compounds **A10** and **A20** had a very similar PK profile. The maximum concentration of **A20** (1.00 nmol/L) was reached on 0.63 h after oral administration; the area under the curve (AUC_{0–24 h}) was

Table 3 Exploration of piperazine derivatives SAR.


Compd.	R ₁	IC ₅₀ (nmol/L) ^a	cLogP ^b	LLE ^c
C1	H	>1000	2.058	—
C2	Ms	0.73 ± 0.41	1.870	7.269
C3	Ac	1.21 ± 1.16	2.08	6.839
C4		1.09 ± 0.68	2.747	6.215
C5		0.89 ± 0.22	3.203	5.846
C6		0.64 ± 0.39	3.665	5.531
C7		0.94 ± 0.37	2.838	6.188
C8		2.66 ± 1.90	2.445	6.131
4	—	0.40 ± 0.25	3.830	5.570
(±)-EC-5026	—	0.09 ± 0.02	4.227	5.825
AR-9281	—	13.8	1.300	6.570

^aThe cell-free IC₅₀ values are recorded on HsEH protein based on biochemical method. The IC₅₀ values were expressed as mean ± standard error of mean (SEM).

^bDiscovery Studio 2016 software was used to predict clogP values.

^cLigand lipophilicity efficiency (LLE) was calculated by following equation: LLE = pIC₅₀ - cLogP.

Table 4 Half-lives of compounds **A10** and **A20** in human and rat microsomal buffer and melting point.

Compd.	Human t _{1/2} (min)	Rat t _{1/2} (min)	Melting point	LLE
A10	69	84	196–198 °C	7.076
A20	174	120	165–166 °C	7.487
4	25	31	204–205 °C	6.570

5.57 nmol h/L; **A20** had a plasma t_{1/2} of 5.18 h. The maximum concentration of **A20** (7.11 nmol/L) was reached on 4.8 min after iv administration; the area under the curve (AUC_{0–12 h}) was 3.90 nmol h/L; **A20** had a plasma t_{1/2} of 6.25 h. The bioavailability of **A20** was 28.6%. However, the maximum concentration of **A10** (0.12 nmol/L) was reached on 2.10 h after oral administration, and bioavailability of **A10** was 3.1%, as shown in **Table 5**. It's worth noting that compound **A10** exhibited high apparent volume of distribution (V_d) and clearance (CL), which demonstrating that **A10** could be widely distributed in the surrounding tissues or bound to plasma proteins as well as quickly metabolized.

The plasma protein binding rate (%PPB) of SD rat was measured through classic equilibrium dialysis devices. The assay disclosed that **A20** showed moderate %PPB (88.6%). Because the therapeutic effect of drug was contributed to the concentration of free drug, this moderate %PPB (88.6%) could be beneficial to analgesic effect *in vivo*.

2.7. Safety of compound **A20**

To further evaluate the potential toxicological effect and adverse events, acute toxicity in Institute of Cancer Research (ICR) mice

Table 5 Pharmacokinetics parameters of **A10** and **A20** in rats after oral and intravenous administration^a.

Parameter	A10 (n = 6)		A20 (n = 6)	
	iv (10 mg/kg)	po (10 mg/kg)	iv (10 mg/kg)	po (50 mg/kg)
T _{max} (h)	0.08	2.10	0.08	0.633
C _{max} (nmol/L)	30.11	0.12	7.11	1.00
t _{1/2} (h)	2.66	2.93	6.25	5.18
CL (mL/h)	749.73	33580.26	1213.60	4070.93
V _z (L)	3.48	224.16	3.683	79.146
AUC _{0–t} (nmol·h/L)	10.14	0.31	3.90	5.57
AUC _{0–∞} (nmol·h/L)	10.20	0.32	3.96	8.02
F (%)	3.1		28.6	

^aAfter administration, blood samples were collected at different time (**A10**: 0, 0.083, 0.17, 0.5, 1, 2, 4, 6, 8, 12 h; **A20**: 0, 0.083, 0.17, 0.33, 0.5, 0.75, 1, 2, 4, 6, 8, 12, 24 h). Compounds formulated in 0.5% CMC-Na solution was administered orally at the indicated doses. The combination of compounds in a ratio of 8% ethanol absolute, 4% Tween-80 and 88% normal saline was chosen for the intravenous injection formulation.

was carried out. The compound **A20** was administered *via po* at a single dose of 6.0 g/kg. Body weight, and behavioral status was continuously recorded for 14 days. According to body weight and apparent behavior problems, no adverse events were observed, indicating that **A20** was well tolerated and had no toxicity at dose of 6.0 g/kg (**Fig. 4**).

In addition, patch clamp technique was performed to detected inhibitory effect of **A20** on human ether-a-go-go related gene (hERG) potassium channels in HEK293 cell lines. Compound **A20** had low hERG activity at 3 μmol/L and 30 μmol/L with inhibitory rates as 0.46% and 41.97%, respectively, which indicating that **A20** couldn't lead to potential adverse effects on heart.

2.8. Pharmacology study of **A20** *in vivo*

Following successful structural optimization of **4**, the behavior of **A20** was further investigated in SD rat with neuropathic pain model induced by spared nerve injury (SNI). The rats were randomly divided into gabapentin (60 mg/kg/day), (±)-EC-5026 (3 mg/kg/day) and **A20** groups, which was further included 1, 3, and 9 mg/kg/day groups. After oral administration with a 12 h dosing interval (BID), mechanical hyperalgesia by von Frey test in rats subjected to evaluate the alleviation of pain on 1, 2, 4, 8, 16, 20 day throughout the study, which was presented as increasing of mechanical paw withdrawal threshold (PWT)³².

Treatment with **A20** was well-tolerated at three doses in SD rats, as shown in **Fig. 5**. On first day, compound **A20** demonstrated significantly analgesic effect at the 3 and 9 mg/kg/day dose levels, both groups were superior to (±)-EC-5026 and gabapentin. At the lowest dose (1 mg/kg/day) tested in this study, treatment with **A20** didn't exhibit significantly analgesic effect. On Day 4, maximum analgesic effect of **A20** at 9 mg/kg/day dose level was achieved. Although the antinociceptive effect of **A20** was weaker than gabapentin before 16 days, the efficacy of gabapentin gradually reduced. Remarkably, on Day 20, antinociceptive effect of **A20** at the 3 and 9 mg/kg/day dose

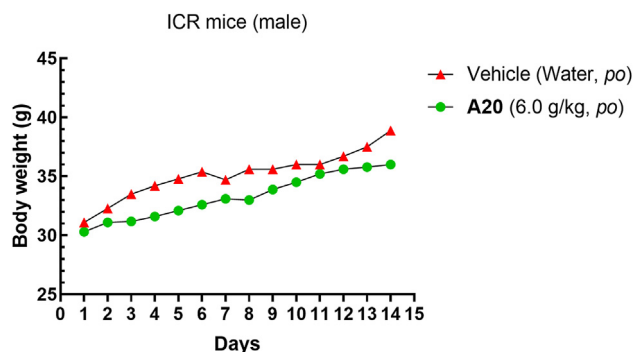


Figure 4 The effect of the compound **A20** on the body weight of ICR mice. **A20** formulated in 0.5% CMC-Na solution was administered orally at the dose of 6.0 g/kg.

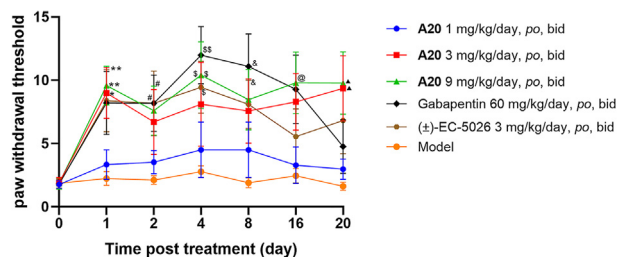


Figure 5 sEH inhibitors attenuate neuropathic pain in SD rat model induced by spared nerve injury. Data are expressed as mean \pm standard error of mean ($n = 6$); * $P < 0.05$, ** $P < 0.01$, vs. Treatment/Model; # $P < 0.05$, vs. Treatment/Model; \$ $P < 0.05$, \$\$\$ $P < 0.01$, vs. Treatment/Model; & $P < 0.05$, vs. Treatment/Model; @ $P < 0.05$, vs. Treatment/Model; ^ $P < 0.05$, vs. Treatment/Model. **A20** formulated in 0.5% CMC-Na solution was administered orally at the indicated doses.

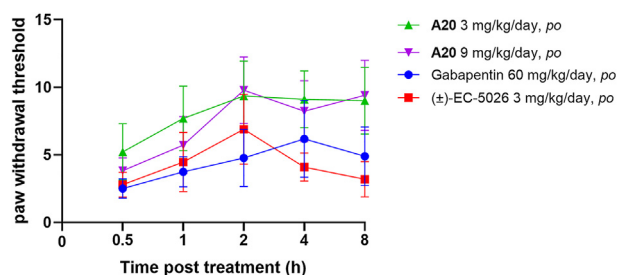


Figure 6 sEH inhibitors attenuate neuropathic pain in rat model induced by spared nerve injury. Data are expressed as mean \pm standard error of mean ($n = 6$).

levels were significantly stronger than (\pm)-EC-5026 and gabapentin. Comparing to the model group, **A20** showed a time- and dose-dependent alleviation of pain and was well tolerated. Treatment with **A20** at dose of 9 mg/kg/day showed best analgesic effect; furthermore, analgesic effect of **A20** at 3 mg/kg/day dose of 3 mg/kg/day was also stronger than (\pm)-EC-5026 and gabapentin. To our delight, the molar dose of **A20** was only 2% of gabapentin.

On Day 20, the time–effect curve of **A20** after last administration was measured, as shown in Fig. 6. At the doses of 3 and 9 mg/kg/day, treatment with **A20** alleviated neuropathic pain for up to 6 h after the last dose in the SNI model, which was significantly longer than

(\pm)-EC-5026 and gabapentin. In addition, **A20** demonstrated faster onset after administration than both positive controls.

3. Conclusions

In summary, we described the identification a new series of memantyl urea derivatives as potent sEH inhibitors, which were derived from an initial lead compound **4** through structure-based rational drug design. Different sites in the lead molecule were systematically optimized, leading to the identification of **A20** as a highly potent sEH inhibitor, which was suitable for evaluating analgesic effect in preclinical neuropathic pain model *in vivo*. The improvement of 1–2 unit LLE was achieved *via* lead modification of piperidinyl to *S*-3-carbamoyl piperidinyl and by the incorporation of F atom at the phenyl group. These events culminated with the discovery of promising molecule **A20**. Oral dosing of **A20** at 3 mg/kg/day in the SD rat with neuropathic pain symptom induced by SNI showed a robust increasing of the PWT level, and analgesic effect of **A20** was stronger than (\pm)-EC-5026 and gabapentin. Delightfully, the molar dose of **A20** is only 2% of gabapentin. According to the promising results obtained with compound **A20**, more research around memantyl urea-containing sEH inhibitors for the treatment of neuropathic pain is currently ongoing.

4. Experimental

4.1. General information

All reagents and starting materials were purchased from commercial suppliers, and used without further purification. Nuclear magnetic resonance (NMR) spectra were obtained on an Ascent 400 MHz spectrometer (^1H frequency of 400 MHz; ^{13}C frequency of 100 MHz). Chemical shifts (δ) are reported in parts per million (ppm) relative to Me_4Si as internal standard. Melting points were determined with an X-4 melting point devices. High-resolution mass spectrometry (HRMS) analysis was performed on an Agilent Technologies 6530 Accurate-Mass Q-TOF MS instrument using electrospray ionization (ESI) as ionization source. Details of compound synthesis and characterization were provided in Supporting Information. The purity analysis of target compounds was carried out by high-performance liquid chromatography (HPLC).

4.2. Biological activity assays *in vitro*

Compounds were screened for their ability to inhibit HsEH by monitoring the hydrolase of (3-phenyloxiranyl)acetic acid cyano(6-methoxynaphthalen-2-yl)methyl ester (PHOME) to corresponding 6-methoxy-2-naphthaldehyde²⁹. The fluorescent assay was performed on purified recombinant HsEH protein. After addition of PHOME solution ($[\text{S}]_{\text{final}} = 50 \mu\text{mol/L}$), the mixture consisted of HsEH protein ($[\text{C}]_{\text{final}} = 6.4 \text{ nmol/L}$) and inhibitor in 25 mmol/L Tris-HCl buffer (pH = 7.4, containing 0.1 mg/mL of BSA) were incubated at 37 °C for 10 min. Fluorescence intensity was read on a SpectraMax M2 instrument at Ex/Em = 330/465 nm. IC_{50} values were measured by regression analysis using IBM SPSS Statistics 20 software.

4.3. Microsomal stability

Hepatic microsomes were commercially obtained from Research Institute for Liver Diseases Co., Ltd. (Shanghai, China). The

detailed experimental procedure followed the procedures reported of our previously work²⁹. The incubation mixture was composed of 490 μL of microsomal protein in 100 mmol/L phosphate buffered saline buffer (pH = 7.4) and 10 μL of **A20** (3.7 mg/mL). The content of human and SD rat's hepatic microsomal protein was 0.4 and 0.53 mg/mL, respectively. NADPH was dissolved in phosphate buffered saline buffer to give 1 mmol/L NADPH solution, which was added to above mixture. After that, the mixture was incubated at 37 °C on 0, 5, 10, 20, 30 and 60 min. Then, the reaction was finished by cool MeCN (500 μL). The resulting mixture was vortexed for 1 min, and EtOAc (400 μL) was added into the mixture (200 μL). The mixture was further vortexed for 1 min, and centrifuged at 3000 rpm for 5 min. After that, supernatant (400 μL) was concentrated with Termovap Sample Concentrator. Then, the residue was reconstituted with 150 μL MeCN:H₂O (7:3, v/v), the resulting mixture was vortexed for 1 min, and centrifuged at 10,000 rpm for 5 min. After that, supernatant was respectively analyzed by HPLC. The concentrations of **A20** were measured by injecting 20 μL of sample onto a reverse-phase WondaSil C18 Superb column (150 mm \times 4.6 mm, 5 μm) at a flow rate of 1 mL/min under the mobile phase conditions: MeCN:H₂O = 70:30 (v/v). Analytical UV detection was recorded at 210 and 230 nm.

4.4. Pharmacokinetics study in vivo

SD rats were used in this study (12 females, 12 males, and 8 weeks old), and purchased from Anhui Medical University (Anhui, China) (License No.: SCXK (Wan) 2017-001). All animal procedures were consisted with the Guiding Principles for Research Involving Animals of Anhui University of Chinese Medicine and all animal experiments were approved by the Animal Ethics Committee of Anhui University of Chinese Medicine (Anhui, China). The SD rats were raised at sterile conditions (18–22 °C, humidity 35%–65%, and ventilation) under daily cycles of light/darkness with a 12 h interval. They went through a period of 3 days of acclimatization before experimental procedure. 24 SD rats were assigned to 4 groups randomly (6 females and 6 males for **A10**; 6 females and 6 males for **A20**). Compounds formulated in 0.5% CMC-Na solution was administered orally at the indicated doses. The combination of compounds in a ratio of 8% ethanol absolute, 4% Tween-80 and 88% normal saline was chosen for the intravenous injection formulation. The SD rats were administered **A10** (10 mg/kg) *via iv* or *po* routes. The SD rats were administered compound **A20** *via iv* or *po* routes with different doses of 10 and 50 mg/kg. SD rats were weighed to calculate the required volume before each administration. Blood samples were obtained at indicated time points (**A10**: 0, 0.083, 0.17, 0.5, 1, 2, 4, 6, 8, 12 h; **A20**: 0, 0.083, 0.17, 0.33, 0.5, 0.75, 1, 2, 4, 6, 8, 12, 24 h). Blood sample was taken from the orbit vein at indicated time points, and collected on eppendorf containing of anticoagulant EDTA-K₂, and centrifuged (4 °C) at 1100 rpm for 5 min. After that, each plasma sample (50 μL) was mixed with tadalafil (50 μL) in MeCN (20 ng/mL) and MeCN (300 μL), resulting mixture was further centrifuged at 13,000 rpm for 10 min. Then, supernatant (50 μL) was reconstituted with MeCN (200 μL), and resulting concentration of compounds were respectively analyzed by TSQ Altis Triple Quadrupole LC/MS instrument (Thermo Scientific). All the pharmacokinetic parameters were obtained using Phoenix WinNonlin software.

4.5. Percentage plasma protein binding (%PPB)

The detailed experimental procedure followed the procedures reported of our previously work²⁹. The experimental assay was calibrated using warfarin of known %PPB: rat plasma (99.5%).

4.6. Efficacy of **A20** in vivo

SD rats were used in this study (males, and 8 weeks old, 180–220 g), and purchased from Jinan Pengyue Experimental Animal Breeding Co., Ltd. (License No.: SCXK (Lu) 20190003). All animal experiments were carried out under the guidelines of the Yantai University Committee for Use and Care of Animals. The animals were raised at sterile conditions (18–22 °C, humidity 35%–65%, and ventilation) under daily cycles of light/darkness with a 12 h interval. They went through a period of 3 days of acclimatization before surgical procedure. The **A20** was suspended in 0.5% carboxymethylcellulose sodium aqueous. All test items were pre-prepared before one day and stored at 4 °C.

Surgical procedure for SD rats with neuropathic pain model induced by spared nerve injury (SNI) was prepared according reported method^{33–35}. The SNI could produce sensory symptoms, such as hypersensitivity to mechanical and thermal stimuli, which develop immediately after 3 days. After successful modeling, rats were randomly divided into vehicle, (\pm)-EC-5026, gabapentin and test groups ($n = 6$). After oral administration with a 12 h dosing interval (BID), mechanical hyperalgesia by von Frey test in rats subjected to evaluate the alleviation of pain throughout the study. On Days 1, 2, 4, 8, 16, 20, PWT of **A20** group was tested. The data was calculated *via* Eq. (1):

$$\text{PWT} = (10^{[k\gamma + k\delta(\text{ppm})]}) / 10,000 \quad (1)$$

Statistical analysis was obtained by GraphPad Prism 8.0.2. Data are expressed as mean \pm standard error of mean.

Acknowledgments

This work was funded by the Liaoning Revitalization Talents Program (XLYC1908031, China), Basic Research Project of Department of Education of Liaoning Province-natural sciences (2020LJC02, China), Major Basic Research Project of Natural Science Foundation of Shandong Province (ZR2018ZC1056, China), and partial support was provided by the NIH-NIEHS RIVER Award (R35 ES030443-01, USA), the NIEHS Superfund Research Program (P42 ES004699, USA).

Author contributions

Fangyu Du: conceptualization, methodology, formal analysis, writing—original draft, writing—review & editing, visualization; Ruolin Cao: visualization, software; Chen Lu: software, investigation; Yajie Shi: resources, investigation; Jianwen Sun: resources, formal analysis; Yang Fu: investigation, validation; Bruce D. Hammock: resources, funding acquisition; Zhonghui: formal analysis, software; Zhongbo Liu: formal analysis, writing—review & editing, funding acquisition, supervision; Guoliang Chen: writing—review & editing, project administration, funding acquisition, supervision. All authors have given approval to the final version of the manuscript.

Conflicts of interest

The authors declare no conflicts of interest.

Appendix A. Supporting information

Supporting information to this article can be found online at <https://doi.org/10.1016/j.apsb.2021.09.018>.

References

- Treede RD, Jensen TS, Campbell JN, Cruccu G, Dostrovsky JO, Griffin JW, et al. Neuropathic pain: redefinition and a grading system for clinical and research purposes. *Neurology* 2008;**70**:1630–5.
- Bouhassira D. Neuropathic pain: definition, assessment and epidemiology. *Rev Neurol (Paris)* 2019;**175**:16–25.
- van Hecke O, Austin SK, Khan RA, Smith BH, Torrance N. Neuropathic pain in the general population: a systematic review of epidemiological studies. *Pain* 2014;**155**:654–62.
- St John SE. Advances in understanding nociception and neuropathic pain. *J Neurol* 2018;**265**:231–8.
- Baron R, Binder A, Wasner G. Neuropathic pain: diagnosis, pathophysiological mechanisms, and treatment. *Lancet Neurol* 2010;**9**:807–19.
- Ji RR, Nackley A, Huh Y, Terrando N, Maixner W. Neuroinflammation and central sensitization in chronic and widespread pain. *Anesthesiology* 2018;**129**:343–66.
- Fiore NT, Austin PJ. Are the emergence of affective disturbances in neuropathic pain states contingent on supraspinal neuroinflammation?. *Brain Behav Immun* 2016;**56**:397–411.
- Song J, Yu H, Liu Y. Current status of treatment and drug discovery for neuropathic pain. *Acta Pharm Sin* 2021;**56**:679–88.
- Shinozaki T, Yamada T, Nonaka T, Yamamoto T. Acetaminophen and non-steroidal anti-inflammatory drugs interact with morphine and tramadol analgesia for the treatment of neuropathic pain in rats. *J Anesth* 2015;**29**:386–95.
- Martinez-Navarro M, Maldonado R, Banos JE. Why mu-opioid agonists have less analgesic efficacy in neuropathic pain. *Eur J Pain* 2019;**23**:435–54.
- Altıparmak B, Cil H, Celebi N. Effect of melatonin on the daytime sleepiness side-effect of gabapentin in adults patients with neuropathic pain. *Rev Bras Anesthesiol* 2019;**69**:137–43.
- Wagner K, Yang J, Inceoglu B, Hammock BD. Soluble epoxide hydrolase inhibition is antinociceptive in a mouse model of diabetic neuropathy. *J Pain* 2014;**15**:907–14.
- Macone A, Otis JAD. Neuropathic pain. *Semin Neurol* 2018;**38**:644–53.
- Gopalsamy B, Farouk AAO, Tengku Mohamad TAS, Sulaiman MR, Perimal EK. Antiallodynic and antihyperalgesic activities of zerrumbone via the suppression of IL-1 β , IL-6, and TNF- α in a mouse model of neuropathic pain. *J Pain Res* 2017;**10**:2605–19.
- Kaspera R, Totah RA. Epoxyeicosatrienoic acids: formation, metabolism and potential role in tissue physiology and pathology. *Expert Opin Drug Metabol Toxicol* 2009;**5**:757–71.
- Wagner KM, Gomes A, McReynolds CB, Hammock BD. Soluble epoxide hydrolase regulation of lipid mediators limits pain. *Neurotherapeutics* 2020;**17**:900–16.
- Morisseau C, Hammock BD. Impact of soluble epoxide hydrolase and epoxyeicosanoids on human health. *Annu Rev Pharmacol* 2013;**53**:37–58.
- Morin C, Sirois M, Echavé V, Albadine R, Rousseau E. 17,18-Epoxyeicosatetraenoic acid targets PPAR γ and p38 mitogen-activated protein kinase to mediate its anti-inflammatory effects in the lung: role of soluble epoxide hydrolase. *Am J Resp Cell Mol* 2010;**43**:564–75.
- Wagner KM, McReynolds CB, Schmidt WK, Hammock BD. Soluble epoxide hydrolase as a therapeutic target for pain, inflammatory and neurodegenerative diseases. *Pharmacol Ther* 2017;**180**:62–76.
- Wagner KM, Atone J, Hammock BD. Soluble epoxide hydrolase inhibitor mediated analgesia lacks tolerance in rat models. *Brain Res* 2020;**1728**:146573.
- Hammock BD, McReynolds CB, Wagner K, Buckpitt A, Cortes-Puch I, Croston G, et al. Movement to the clinic of soluble epoxide hydrolase inhibitor EC5026 as an analgesic for neuropathic pain and for use as a nonaddictive opioid alternative. *J Med Chem* 2021;**64**:1856–72.
- Chiamvimonvat N, Ho CM, Tsai HJ, Hammock BD. The soluble epoxide hydrolase as a pharmaceutical target for hypertension. *J Cardiovasc Pharmacol* 2007;**50**:225–37.
- Imig JD, Zhao X, Capdevila JH, Morisseau C, Hammock BD. Soluble epoxide hydrolase inhibition lowers arterial blood pressure in angiotensin II hypertension. *Hypertension* 2002;**39**:690–4.
- Chen D, Whitcomb R, MacIntyre E, Tran V, Do ZN, Sabry J, et al. Pharmacokinetics and pharmacodynamics of AR9281, an inhibitor of soluble epoxide hydrolase, in single- and multiple-dose studies in healthy human subjects. *J Clin Pharmacol* 2012;**52**:319–28.
- Wang L, Yang J, Guo L, Uyeminami D, Dong H, Hammock BD, et al. Use of a soluble epoxide hydrolase inhibitor in smoke-induced chronic obstructive pulmonary disease. *Am J Respir Cell Mol Biol* 2012;**46**:614–22.
- Lazaar AL, Yang L, Boardley RL, Goyal NS, Robertson J, Baldwin SJ, et al. Pharmacokinetics, pharmacodynamics and adverse event profile of GSK2256294, a novel soluble epoxide hydrolase inhibitor. *Br J Clin Pharmacol* 2016;**81**:971–9.
- Mao J, Gold MS, Backonja MM. Combination drug therapy for chronic pain: a call for more clinical studies. *J Pain* 2011;**12**:157–66.
- Lee KSS, Ng JC, Yang J, Hwang SH, Morisseau C, Wagner K, et al. Preparation and evaluation of soluble epoxide hydrolase inhibitors with improved physical properties and potencies for treating diabetic neuropathic pain. *Bioorg Med Chem* 2020;**28**:115735.
- Du F, Sun W, Morisseau C, Hammock BD, Bao X, Liu Q, et al. Discovery of memantinyll urea derivatives as potent soluble epoxide hydrolase inhibitors against lipopolysaccharide-induced sepsis. *Eur J Med Chem* 2021;**223**:113678.
- Wolf NM, Morisseau C, Jones PD, Hock B, Hammock BD. Development of a high-throughput screen for soluble epoxide hydrolase inhibition. *Anal Biochem* 2006;**355**:71–80.
- Leeson P, Springthorpe B. The influence of drug-like concepts on decision-making in medicinal chemistry. *Nat Rev Drug Discov* 2007;**6**:881–90.
- Chaplan SR, Bach FW, Pogrel JW, Chung JM, Yaksh TL. Quantitative assessment of tactile allodynia in the rat paw. *J Neurosci Methods* 1994;**53**:55–63.
- Guida F, De Gregorio D, Palazzo E, Ricciardi F, Boccella S, Belardo C, et al. Behavioral, biochemical and electrophysiological changes in spared nerve injury model of neuropathic pain. *Int J Mol Sci* 2020;**21**:3396.
- Boccella S, Guida F, Palazzo E, Marabese I, de Novellis V, Maione S, et al. Spared nerve injury as a long-lasting model of neuropathic pain. *Methods Mol Biol* 2018;**1727**:373–8.
- Jin X, Luo A, Zhang G. Comparison of the establishment and efficacy of three neuropathic pain models. *J Clin Anesth* 2005;**21**:338–40.